Computers and Mathematics with Applications 163 (2024) 42–55

Contents lists available at ScienceDirect

Computers and Mathematics with Applications

journal homepage: www.elsevier.com/locate/camwa

Directional enrichment functions for finite element solutions of transient anisotropic diffusion

Abderrahim Bahssini [a], Nouh Izem [a], M. Shadi Mohamed [b,c,*], Mohammed Seaid [d]

[a] Laboratory of Mathematical Engineering and Computer Science, Faculty of Science, Ibn Zohr University Agadir, Morocco
[b] School of Energy, Geoscience, Infrastructure and Society, Heriot-Watt University, Edinburgh, United Kingdom
[c] State Key Laboratory of Mechanics and Control of Mechanical Structures, Nanjing University of Aeronautics and Astronautics, Nanjing 210016, China
[d] Department of Engineering, University of Durham, South Road, Durham DH1 3LE, United Kingdom

ARTICLE INFO

Keywords:
Anisotropic diffusion
Transient problems
Partition of unity method
Finite element method
Directional enrichment

ABSTRACT

The present study proposes a novel approach for efficiently solving an anisotropic transient diffusion problem using an enriched finite element method. We develop directional enrichment for the finite elements in the spatial discretization and a fully implicit scheme for the temporal discretization of the governing equations. Within this comprehensive framework, the proposed class of exponential functions as enrichment enhance the approximation of the finite element method by capturing the directional based behaviour of the solution. The incorporation of these enrichment functions leverages a priori knowledge about the anisotropic problem using the partition of unity technique, resulting in significantly improved approximation efficiency while retaining all the advantages of the standard finite element method. Consequently, the proposed approach yields accurate numerical solutions even on coarse meshes and with significantly fewer degrees of freedom compared to the standard finite element methods. Moreover, the choice of mesh coarseness remains independent of the anisotropy in the problem, enabling the use of the same mesh regardless of changes in the anisotropy. Using extensive numerical experiments, we consistently demonstrate the efficiency of the proposed method in attaining the desired levels of accuracy. Our approach not only provides reliable and precise solutions but also extends the capabilities of the finite element method to effectively address aspects of the heterogeneous anisotropic transient diffusion problems that were previously considered ineffective when using this method.

1. Introduction

In general, the diffusion equation describes the behaviour of the concentration of microparticles, molecules, or microorganisms as they strive to reach equilibrium in a surrounding environment. It can also represent the heat conduction in a medium and the diffusive behaviour strongly depends on the properties of the surrounding environment or participating medium. In many highly relevant cases, the diffusivity changes with the direction inside the medium. In fact, differences between directions can span several orders of magnitude and this behaviour, known as anisotropic diffusion, can be observed in biological processes [54,56], hydrological processes [35], and geological processes [66]. A well-established example is found in the plasma fusion for which the thermal conductivity or diffusion coefficient can be up to 10^{12} times higher in certain directions compared to others [65]. In these cases, the numerical solution of anisotropic diffusion problems can be computationally challenging because the accuracy of the solution highly depends on mesh alignment [46,17,64]. Even local misalignments can cause severe computational issues related to numerical instabilities [10]. For instance, errors in the direction of the highest diffusion can significantly increase the numerical error in all other directions [65]. To reduce the numerical diffusion, higher-order finite elements are used in the direction of the largest diffusivity [62,48,33] and therefore, non-uniform meshes are employed. The multipoint flux approximation is a cell-centred finite volume method that can provide stability and it preserves local conservation when considering a discontinuous diffusion tensor [1,2,25]. Different variations of the multipoint flux approximation have been developed for nonlinear [14] and heterogeneous [30] anisotropic problems. In these approaches, the flux continuity must be evaluated and satisfies a continuity condition on

* Corresponding author at: School of Energy, Geoscience, Infrastructure and Society, Heriot-Watt University, Edinburgh, United Kingdom.
E-mail address: m.s.mohamed@hw.ac.uk (M.S. Mohamed).

https://doi.org/10.1016/j.camwa.2024.03.016
Received 18 July 2023; Received in revised form 9 February 2024; Accepted 10 March 2024

each element edge and, in some cases, on the domain boundaries as well, which can impact the computational efficiency of the method [68]. Various schemes have also been proposed to approximate the fluxes, but in general, maintaining accuracy at extreme anisotropy levels is difficult due to the non-symmetric nature of the diffusion operator [57]. To improve the accuracy, dual-grid methods such as the discrete duality finite-volume method [4] have been proposed. Although this method can achieve a convergence rate better than first-order, the mesh remains anisotropy-dependent, as reported for coarse meshes [41]. The hybrid finite volume method [29], the mixed finite volume method [23,24], and the monotone finite volume method [43,67] are other finite volume techniques that rely on dual meshes. Furthermore, these methods require the implementation of positivity-preserving mechanisms in the discrete systems so that they are not dependent on the implemented solver [63]. In general, all the discussed finite volume methods treat the mathematical operator exactly while approximating the constitutive relations [65]. The same observation is also made in the mimetic spectral element method for anisotropic diffusion problems [7]. Another approach proposed for severely anisotropic problems is to split the problem using asymptotic preserving schemes into two parts namely, a limit problem for infinite anisotropy and a singular perturbation problem [15,16]. This approach is extended to unsteady anisotropic diffusion problems in [65] and later, limiters are imposed to avoid non-physical negative energy [40,58]. A comprehensive review of the work carried out on asymptotic preserving schemes can be found in [39,37]. However, it should be noted that the majority of the asymptotic preserving schemes studied in the literature are restricted to one-dimensional problems and/or structured meshes [5]. To overcome these restrictions, discontinuous finite element methods [9,3] or Trefftz discontinuous Galerkin methods [8] are employed. Compared to continuous approaches, the discontinuous Galerkin method has the advantage of flexible adaptivity. In this context, the control volume finite element method is proposed [55]. Here, an accurate across-face flux is maintained using a least square method. The control volume finite element method combines the flexibility of finite elements with the control volume efficiency in the conservation of transported properties [11]. Different discontinuous Galerkin methods are discussed in [36], while a hybrid discontinuous scheme is presented in [32]. However, discontinuous approaches can often result in ill-conditioned linear systems that worsen at high anisotropy.

To overcome the difficulties mentioned above, we propose enriching the finite element method with a set of special functions accounting for the anisotropy in the problem under study. The proposed enrichment method is based on the partition of unity method initially proposed in [49] and later developed for the diffusion problems in the context of the partition of unity finite element method [50]. It has since been extended to conduction-radiation problems [51] and nonlinear diffusion equations [45]. The enrichment approach is also employed to solve the inverse diffusion problems [38]. The advantages include not only coarse meshes that are independent of the problem but also a significant reduction in the computational time by increasing numerical efficiency [52,44]. A comprehensive framework for enhancing finite element approximations through additional enrichment functions establishing the validity of the finite element method can be found in [34] among others. Furthermore, non-polynomial basis functions have also been shown to enhance the standard simplicial linear finite element, see for example [18,19].

The key idea in the present study is to enrich the finite element approximation space with exponential functions that reflect the diffusion behaviour [20]. For example, the enrichment functions can have steep gradients to efficiently capture any boundary layers without the need for highly refined elements on the domain boundary [61,45], or they can be time-dependent to continuously adapt with the time [31]. In this work, we construct enrichment functions using the fundamental solutions of the anisotropic diffusion equations and the partition of unity method. By incorporating such a priori knowledge on the diffusion problem into the finite element approximation, the resulting high-order basis functions can best describe the anisotropy without imposing any restrictions on the mesh. The proposed method is fully continuous, avoiding any shortcoming associated with discontinuous elements. Furthermore, the approach inherits the full flexibility of the finite element method in dealing with general geometries and heterogeneous computational domains. To validate and assess the efficiency of the proposed method, we compare the results to those obtained using the conventional finite element method.

The rest of this paper is organized as follows. In section 2 we introduce the anisotropic transient diffusion problems considered in this work. The formulation of the proposed method is presented in section 3. This section defines the space discretization along with the directional enrichment functions includes and the time integration scheme used in the current study. Section 4 is devoted to numerical results using several test examples of anisotropic transient diffusion problems. Comparisons between numerical results obtained using the proposed partition of unity finite element method and those obtained using the conventional finite element method are also included in this section. In section 5 we summarize the conclusions and propose some recommendations for further work.

2. Anisotropic transient diffusion problem

In the present study, we consider anisotropic diffusion problems described by the following two-dimensional model [28]

$$\frac{\partial u}{\partial t} - \nabla \cdot (\mathbf{K}\nabla u) = f(t,\mathbf{x}), \qquad (t,\mathbf{x}) \in (0,T]\times\Omega, \tag{1}$$

where Ω is a bounded spatial domain with boundary $\partial\Omega$, $(0,T]$ is the time interval, $u(t,\mathbf{x})$ represents the temperature in a heat transfer problem or the pressure in a transport problem in porous media, t denotes the time, $\mathbf{x} = (x,y)^\top$ the space coordinates, $f(t,\mathbf{x})$ is a source term, and $\mathbf{K}$ the diffusion tensor which may depend on the space and time as well. Here, the unit direction vector $\mathbf{b} = (\cos\alpha, \sin\alpha)^\top$ represents the misalignment of the grid with α is the misalignment angle. For a two-dimensional problem, the diffusion tensor is defined by $\mathbf{K} = \mathcal{R}\Lambda\mathcal{R}^\top$, with the rotation matrix given as

$$\mathcal{R} = \begin{pmatrix} \cos\alpha & -\sin\alpha \\ \sin\alpha & \cos\alpha \end{pmatrix},$$

and $\Lambda = \mathrm{diag}(K_\parallel, K_\perp)$, with $K_\parallel$ and $K_\perp$ represent the parallel and perpendicular diffusion coefficients, respectively. Hence, the diffusion tensor can be formulated as

$$\begin{aligned}\mathbf{K} &= \begin{pmatrix} K_{xx} & K_{xy} \\ K_{yx} & K_{yy} \end{pmatrix} \\ &= \begin{pmatrix} K_\parallel \cos^2(\alpha) + K_\perp \sin^2(\alpha) & \frac{1}{2}\left(K_\parallel - K_\perp\right)\sin(2\alpha) \\ \frac{1}{2}\left(K_\parallel - K_\perp\right)\sin(2\alpha) & K_\parallel \sin^2(\alpha) + K_\perp \cos^2(\alpha) \end{pmatrix}.\end{aligned} \tag{2}$$

Notice that the diffusion tensor $\mathbf{K}$ is positive definite and symmetric, satisfying $K_{xx}K_{yy} - K_{yx}K_{xy} > 0$. We also define the anisotropy ratio as $\varsigma = \frac{K_\parallel}{K_\perp}$. In addition, we assume the diffusion equation is equipped with following boundary and initial conditions

$$\mathbf{K}\nabla u \cdot \mathbf{n} + u = g(t,\mathbf{x}), \qquad (t,\mathbf{x}) \in (0,T]\times\partial\Omega, \tag{3}$$

$$u(0,\mathbf{x}) = u_0(\mathbf{x}), \qquad \mathbf{x}\in\Omega, \tag{4}$$

where $\mathbf{n}$ is the outward normal vector on $\partial\Omega$, $g(t,\mathbf{x})$ and $u_0(\mathbf{x})$ are given boundary and initial functions, respectively. It should be noted that we are limited to linear problems and therefore, only constant values of the diffusion tensor $\mathbf{K}$ are considered in the present study.

To solve the boundary-value problem defined by (1)-(4), we divide the time interval $[0,T]$ into N subintervals $\left[t_n, t_{n+1}\right]$ with a timestep $\Delta t = t_{n+1} - t_n$ for $n = 0,1,\ldots,N$. We also use the notation $w^n(\mathbf{x})$ to denote the approximation of a generic function $w(t,\mathbf{x})$ at time t_n. We also

discretize the spatial domain ω into a finite set of conforming elements $\mathcal{T}_j$ ($j = 1, 2, \dots N_e$) with N_e is the total number of elements. Recall that a method is considered to be "conforming" when the finite element space is a subset of the solution space. In such cases, it is well-established that the approximative finite element solution converges to the true solution, as long as the finite element space appropriately approximates the given space, see for instance [60]. Here, the computational domain $\Omega_h \subseteq \Omega$ is the combination of all these finite elements. Applied to the diffusion equation (1), the implicit Euler scheme for time integration yields

$$\frac{u^{n+1} - u^n}{\Delta t} - \nabla \cdot \left(\mathbf{K} \nabla u^{n+1}\right) = f^{n+1}. \tag{5}$$

Multiplying by an arbitrary test function v, integrating over Ω and using Green's theorem [50,47], one obtains

$$\int_\Omega \nabla \cdot \left(\mathbf{K} \nabla u^{n+1}\right) v \, d\mathbf{x} = \oint_{\partial\Omega} \mathbf{K} \nabla u^{n+1} \cdot \mathbf{n} v \, d\mathbf{x} - \int_\Omega \mathbf{K} \nabla u^{n+1} \cdot \nabla v \, d\mathbf{x}. \tag{6}$$

We then define the following weak formulation: find $u^n \in H^1(\Omega)$ such that

$$\begin{aligned} &\int_\Omega u^{n+1} v \, d\mathbf{x} + \Delta t \int_\Omega \left(\frac{\partial v}{\partial x} \left(K_{xx} \frac{\partial u^{n+1}}{\partial x} + K_{xy} \frac{\partial u^{n+1}}{\partial y} \right) \right. \\ &\left. + \frac{\partial v}{\partial y} \left(K_{yx} \frac{\partial u^{n+1}}{\partial x} + K_{yy} \frac{\partial u^{n+1}}{\partial y} \right) \right) d\mathbf{x} - \Delta t \oint_{\partial\Omega} \mathbf{K} \nabla u^{n+1} \cdot \mathbf{n} v \, d\mathbf{x} \\ &= \Delta t \int_\Omega f^{n+1} v \, d\mathbf{x} + \int_\Omega u^n v \, d\mathbf{x}, \end{aligned} \tag{7}$$

where $H^1(\Omega)$ denotes the standard Sobolev space. We also define the conforming finite element space V_h as

$$V_h = \left\{ u_h \in C^0(\overline{\Omega}) : \quad u_h\Big|_{\mathcal{T}} \in \mathcal{P}_m(\mathcal{T}), \quad \forall\, \mathcal{T} \in \Omega_h \right\}, \tag{8}$$

with

$$\mathcal{P}\left(\mathcal{T}_j\right) = \left\{ p(\mathbf{x}) : \quad p(\mathbf{x}) = \hat{p} \circ Y_k^{-1}, \quad \hat{p} \in P_m \right\}, \tag{9}$$

where P_m is the set of polynomials of degree $\leq m$. The polynomial $\hat{p}(\mathbf{x})$ is defined on the element $\hat{\mathcal{T}}_j$ and Y_k is an invertible one-to-one mapping between the element $\hat{\mathcal{T}}_j$ and the reference element. Here, the average element size h represents the typical size or the largest side of the elements $\hat{\mathcal{T}}_j$ used in discretizing a domain, and it significantly influences the accuracy and convergence of the numerical solution. Note that smaller values of h result in finer and more accurate meshes but they require increased computational resources, while larger values of h yield coarser and computationally demanding meshes but with potential trade-offs in the accuracy. The approximated solution using the conventional finite element method is given by

$$u_h^n(\mathbf{x}) = \sum_{i=1}^{M} U_i^n \phi_i(\mathbf{x}), \tag{10}$$

where M is the number of solution mesh points in the partition Ω_h and U_i^n are the unknown nodal solutions to be calculated. Note that the set $\left\{\phi_i\right\}_{i=1}^M$ forms a basis of V_h with $\phi_i \in V_h$ and $\phi_i\left(\mathbf{x}_j\right) = \delta_{ij}$ for $i, j = 1, \dots, M$, where δ_{ij} is the canonical Kronecker delta. Thus, the conventional approximation space is defined as

$$\widetilde{V}_h^0 = \text{span}\left\{ \phi_h, \quad U_h = \sum_{i=1}^{M} U_i^n \phi_i \right\}. \tag{11}$$

To enhance the finite element approximation (10) which is based on polynomial basis functions, we present in the next section a methodology to enrich the solution space (11) with a set of exponential basis functions accounting for the anisotropic nature of the considered diffusion problem (1).

3. Directional enrichment functions

In the present study, to improve the conventional finite element approximation (10) which is based on polynomials, we enrich the finite element space with a class of Gaussian functions. The directional enrichment functions are proposed based on the fundamental solution to have better approximation properties for solving the diffusion equations with anisotropic coefficients as those considered in this work. It should be noted that the partition of unity finite element method is selected because it ensures inter-element continuity in a straightforward manner which simplifies its implementation in any existing finite element software with minimal changes. Here, to account for anisotropy, the following sum of anisotropic exponential functions are used to enrich the solution space

$$F_{\text{enr}} = \left\{ G_1, G_2, \dots, G_Q \right\}, \tag{12}$$

with

$$G_q(\mathbf{x}) = \frac{\exp\left(-\left(\frac{\sqrt{\det(\mathbf{K}) \widetilde{\mathbf{x}}^\top \mathbf{K}^{-1} \widetilde{\mathbf{x}}}}{C} \right)^q \right) - \exp\left(-\left(\frac{R}{C} \right)^q \right)}{1 - \exp\left(-\left(\frac{R}{C} \right)^q \right)},$$

$$q = 1, 2, \dots, Q, \tag{13}$$

where Q is the total number of enrichment functions and $\widetilde{\mathbf{x}} = \mathbf{x} - \mathbf{x}_0$, with $\mathbf{x}_0 = (x_0, y_0)^\top$ are control points placed in a region of the computational domain with a zero or a minimum gradient such that the gradient increases in any direction inside the domain and away from these control points. Note that in most diffusion problems, the region of the domain with zero-gradient is often within the domain core far from the source terms. In the enrichment functions (13), $\mathbf{K}$ the diffusion tensor provide the directional behaviour of the enrichment while the exponent q, the parameters C and R are introduced to control the gradient of the sum of the exponential functions G_q in the anisotropy directions. In a parametric study performed in this work and not presented here for brevity in the presentation, a value range of $[1, 5]$ for the parameter C and $R \approx 2C^2$, leads to the best performance of the proposed enrichment. For illustration, the functions G_q, with $q = 1, 2, \dots, 8$ and three different misalignment angles, are depicted and compared in Fig. 1. The figure shows the impact of the exponent q and the angle α on the enrichment functions. The former changes the steepness of the function while the latter leads to anisotropic behaviour of the enrichment functions. Note that it is possible to optimize the parameters q, C and R for each specific diffusion problem under study, but such optimization procedure has a limited impact on the performance of enrichments as long as these constants remain within the above mentioned range. However, selecting these parameters to be an order of magnitude different may lead to inaccuracies for the enriched finite element approximation. It is also worth noting that for isotropic diffusion problems, the directional enrichment functions (13) reduce to a set of simple exponential functions similar to those functions first introduced in [50] for solving the isotropic diffusion equations. Notice that the sum of multiple functions G_q with $q = 1, 2, \dots, Q$ can be considered as a generalization of the exponential functions considered in previous work so that the time-dependency of the anisotropic enrichment is avoided.

Hence, the anisotropic enrichment is included in the finite element approximation by expanding the nodal values to be rewritten as

$$U_j^n = \sum_{q=1}^{Q} A_{j,q}^n G_q(\mathbf{x}). \tag{14}$$

Note that a global enrichment approach is adopted in this work such that the same directional enrichment functions are applied at all nodes in the computational domain. The inter-element C^0 continuity is naturally ensured using the partition of unity finite element method. In addition, the implementation of the approach in already existing finite

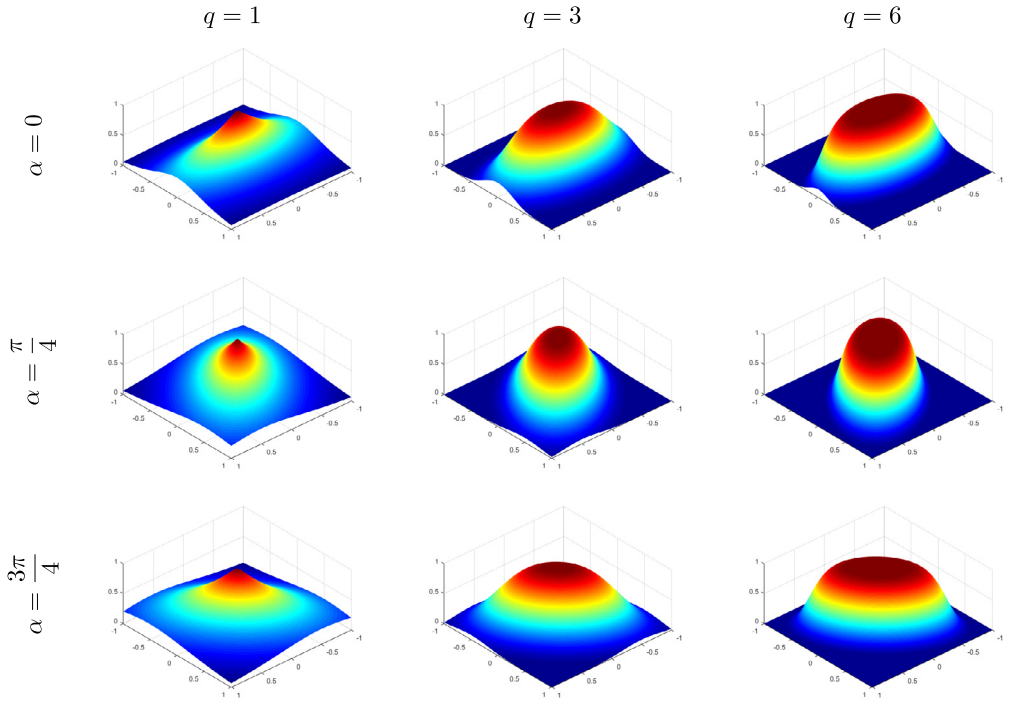

Fig. 1. Illustration of the directional enrichment functions G_q for different values of q and α.

element codes would require minimal changes. It is also evident that the finite element method is now used to find the values of the new set of unknowns $A^n_{j,q}$ instead of the nodal values U^n_j as in the conventional finite element method. Inserting (14) in (10), one obtains

$$u^n_h(\mathbf{x}) = \sum_{j=1}^{M}\sum_{q=1}^{Q} A^n_{j,q}\phi_j(\mathbf{x})G_q(\mathbf{x}). \tag{15}$$

For simplicity, the multiplication of the polynomial shape functions ϕ_j by the enrichment functions G_q is considered to be the new shape function $L_{(j-1)Q+q}$ and denoted as

$$L_{(j-1)Q+q}(\mathbf{x}) = \phi_j(\mathbf{x})G_q(\mathbf{x}), \tag{16}$$

and the new approximation space becomes

$$\widetilde{V}^1_h = \text{span}\left\{ L_h, \qquad U_h = \sum_{j=1}^{M}\sum_{q=1}^{Q} A^n_{j,q} L_{(j-1)Q+q} \right\}. \tag{17}$$

It should be stressed that the new shape functions (16) are composed of the directional enrichment functions $G_q(\mathbf{x})$ which are written in terms of the global coordinates $\mathbf{x}$ multiplied by the nodal polynomial shape functions $\phi_j(\mathbf{x})$. These new shape functions have different approximation properties at different elements based on the behaviour of the global enrichment functions in these elements. The global approximations are made local in the vicinity of a feature of interest such as steep internal or boundary layers using the local basis functions. Injecting the approximation (15) in the weak formulation (7) yields the following system of algebraic equations to be solved at each timestep

$$\left[[\mathbf{M}] + \frac{1}{\Delta t}[\mathbf{S}]\right]\{\mathbf{a}^n\} = \{\mathbf{b}^n\}, \tag{18}$$

where the set of unknowns $A^n_{j,q}$ is assembled into the vector $\mathbf{a}^n$ which has MQ entries, $[\mathbf{M}]$ and $[\mathbf{S}]$ are respectively, the $MQ \times MQ$-valued mass and stiffness matrices the entries of which are M_{qr} and S_{qr} defined by

$$M_{qr} = \int_\Omega \left(\frac{\partial L_r}{\partial x}\left(K_{xx}\frac{\partial L_q}{\partial x} + K_{xy}\frac{\partial L_q}{\partial y}\right) + \frac{\partial L_r}{\partial y}\left(K_{yx}\frac{\partial L_q}{\partial x} + K_{yy}\frac{\partial L_q}{\partial y}\right)\right) d\mathbf{x} - \oint_{\partial\Omega} \mathbf{K}\nabla L_q \cdot \mathbf{n} L_r \, d\mathbf{x}, \tag{19}$$

$$S_{qr} = \int_\Omega L_r L_q \, d\mathbf{x},$$

and $\{\mathbf{b}^n\}$ is the MQ-valued vector of the force term the entries of which are

$$b^n_s = \int_\Omega f^{n+1} L_s \, d\mathbf{x} + \frac{1}{\Delta t}\int_\Omega U^n L_s \, d\mathbf{x}. \tag{20}$$

It should be mentioned that the resulting linear system (18) may suffer from conditioning issues particularly when increasing the number of enrichment functions. This has been well documented in the literature, see for example [50]. This behaviour is often attributed to the similarities between the enrichment functions as the number of these functions increases. To overcome this challenge in the present study, we have limited the maximum number of enrichment functions to six (*i.e.* $Q = 6$). Furthermore, the resulting linear systems of algebraic equations are solved using a direct solver. However, it should also be pointed out that various iterative solvers and pre-conditioning strategies are also possible to use with the proposed method as discussed in [53,22].

The solution of the transient anisotropic diffusion problem (1)-(4), can have steep gradients and fronts moving within the time. Similarly, the enrichment functions have steep gradients at different locations in the computational domain so that they accurately represent the solution at different stages in time. This feature would help to capture the solution steep gradients and fronts as they move in the domain, and this variation in time is well captured by the sum of enrichment functions although these functions are time-independent. Note that other enrichment functions including time-dependent functions can also be used in our approach without major conceptual modifications. Moreover, the main advantage of the time-independent enrichment functions is the possibility to build the assembled matrix for the linear system (18) only at the first timestep to be used in subsequent timesteps. In addition, since only the right-hand side of the linear system (18) is updated in the time integration process, one may factorize the matrix using an LU decomposition at the first timestep and the solution is computed us-

ing backward/forward substitutions. This can significantly increase the efficiency when a large number of timesteps is needed compared to updating the matrix and fully solving the system at every timestep. Recent studies such as those published in [12,27,21] have explored the computational performance of the partition of unity enriched elements in comparison to high-order polynomial-based finite elements. Notably, these comparisons have been conducted in the context of heat transfer [27] and wave problems [12,21]. The results reported in these references consistently demonstrated a significant advantage for the enriched finite element method in terms of reducing the number of degrees of freedom required for accurate solutions. It is acknowledged that the enriched finite element method may encounter challenges related to ill-conditioned systems when compared to the traditional finite element methods. Comparatively, while increasing the polynomial order hierarchically allows for adaptive mesh refinement and enhanced accuracy, high-order finite element methods often demand tailored mesh designs specific to their polynomial orders. It is evident that not all high-order finite element methods exhibit the same sensitivity to element quality [26,42]. For example, some problems show good agreement in stiffness matrix condition numbers for different methods, while discrepancies are observed in others, emphasising the need for a nuanced understanding of shape functions and element distortion [42]. Moreover, ongoing efforts in mesh adaptation strategies, such as the log-simplex method, aim to enhance the robustness and accuracy of high-order elements [13]. These findings highlight the importance of considering the nuances of different high-order finite elements in ensuring mesh quality.

Our approach, employing low-order enriched elements within the enriched finite element method, offers simplicity and generality during mesh generation. It bypasses the need for tailored high-order mesh designs and remains effective even on relatively poor-quality elements, as observed in numerical examples found in reference [53]. This ensures ease of implementation and reduces user involvement in mesh generation. Considering these findings, we anticipate a similar trend in our study when comparing the proposed anisotropic enriched finite element method with high-order finite element methods. Needless to mention that, while being mindful of the conditioning issues, we believe that our approach strikes a practical balance between computational efficiency and accuracy. Furthermore, the integrals appearing in (19) and (20) are evaluated numerically using the standard Gauss-Legendre quadrature. We ensured in all presented numerical results that the chosen number of quadrature points is high enough to eliminate the effect of integration errors. Although usually the number of integration points per element is much higher with the proposed partition of unity finite element method than with the conventional finite element method, the total number of integration points in the entire domain with the proposed method is smaller to that of the corresponding number of the conventional method. This is mainly due to the much higher number of elements needed for the conventional finite element method compared to the partition of unity finite element method.

4. Numerical results and examples

To evaluate the performance of the proposed Anisotropic Partition of Unity Finite Element Method (Aniso-PUFEM), we conduct various numerical simulations for anisotropic diffusion problems. Firstly, we consider an anisotropic transient diffusion equation with known analytical solutions. This example enables us to quantify errors in our numerical solutions and compare the effectiveness of our enrichment technique with the Gaussian-based enrichment available in the literature [50], as well as with the standard Finite Element Method (FEM). Subsequently, we apply the Aniso-PUFEM to solve transient anisotropic diffusion problems within different enclosures and considering localized sources. Throughout all our simulations, we compare the results obtained for the Aniso-PUFEM on an Intel(R) Core(TM) i3 CPU clocked at 2.27 GHz, equipped with 4 GB of RAM using Fortran 95 for sequential coding. These tests provide insights into the accuracy and efficiency of the Aniso-PUFEM in tackling anisotropic diffusion problems using unstructured meshes and different enrichment options.

4.1. Accuracy test problem

In this first example, we employ the Aniso-PUFEM to solve the anisotropic transient diffusion problem (1) in a squared domain $\Omega = [-1,1]\times[-1,1]$. The following exact solution is imposed for this test problem

$$\begin{aligned} u(t,x,y) = \left(\frac{5}{3}\right)^7 \left(1-e^{-10t}\right)\left(1-x^2\right)\left(1-y^2\right) \\ \times\left(6-x^2\left(K_{\parallel}\sin^2(\alpha)+K_{\perp}\cos^2(\alpha)\right)\right. \\ +2xy\left(\frac{1}{2}\left(K_{\parallel}-K_{\perp}\right)\sin(2\alpha)\right) \\ \left.-y^2\left(K_{\parallel}\cos^2(\alpha)+K_{\perp}\sin^2(\alpha)\right)\right)^7. \end{aligned} \tag{21}$$

Note that the source term $f(t,x,y)$, the boundary function $g(t,x,y)$, and the initial condition $u_0(x,y)$ are explicitly calculated based on this analytical solution (21). In our simulations for this example, the misalignment angle is set to $\alpha = \frac{\pi}{4}$ as specified in [6], while the diffusion coefficients are chosen as $K_{\perp} = 1$ and $K_{\parallel} = 3$. It is important to note that to prevent the exact solution (21) from being a subset of the enrichment space (17), the analytical solution is manufactured using multiplicative polynomials and trigonometric functions in the spatial domain. Here, we solve the problem using the partition unity finite element method with two enrichment options. The first option utilizes the proposed directional enrichment functions (13) and referred to as Aniso-PUFEM, while the second option involves using the canonical Gaussian functions initially proposed for isotropic media in [50]. This latter approach is referred to as Iso-PUFEM. In addition, this problem is solved using the conventional finite element method.

In Fig. 2, we illustrate the unstructured meshes used for this example. Here, a coarse mesh (Mesh 1) composed of 67 elements and 44 nodes is used for the Aniso-PUFEM and Iso-PUFEM, and a fine mesh (Mesh 2) of 12442 elements and 6363 nodes is used for the FEM. The considered finite elements in both meshes are linear three-noded elements. All the integrals are evaluated using the Gaussian quadrature and the number of integration points has been increased until the integration has converged for the PUFEM solutions. A direct solver is used to solve the resulting linear system of equations. The main aim of this test example is to compare the results obtained using the Aniso-PUFEM to those obtained using the Iso-PUFEM on the coarse mesh and to those obtained using the FEM on the fine mesh. The three methods are compared using the relative L^2-error norm defined as

$$L^2\text{-error} = \frac{\|u_h - u\|_{L^2(\Omega)}}{\|u\|_{L^2(\Omega)}}, \tag{22}$$

where $\|\cdot\|_{L^2(\Omega)}$ represents the L^2-norm, U_h is the computational solution and U is the exact solution.

Table 1 summarizes the errors obtained using the Iso-PUFEM, Aniso-PUFEM, and FEM on the considered meshes at the final time $t = 10^{-3}$ using a timestep $\Delta t = 10^{-5}$. The relative errors obtained using Aniso-PUFEM and Iso-PUFEM for an increased number of enrichment functions are also presented in this table. Using the same number of enrichment functions, the proposed Aniso-PUFEM achieves an order of magnitude improvement in the error compared to the Iso-PUFEM. For example, with only 132 degrees of freedom, the Aniso-PUFEM achieves an error of 8.30E-03 at the final time compared to an error of 7.47E-02 using the Iso-PUFEM. The better accuracy is attributed to the anisotropic enrichment functions that can better reflect the problem behaviour compared to enriching with the generic Gaussian functions. To further explain the impact of the enrichment, we show in Fig. 3 snapshots of the exact solution and the numerical solutions obtained using Aniso-PUFEM and Iso-PUFEM on the coarse mesh at $t = 10^{-3}$. It is clear

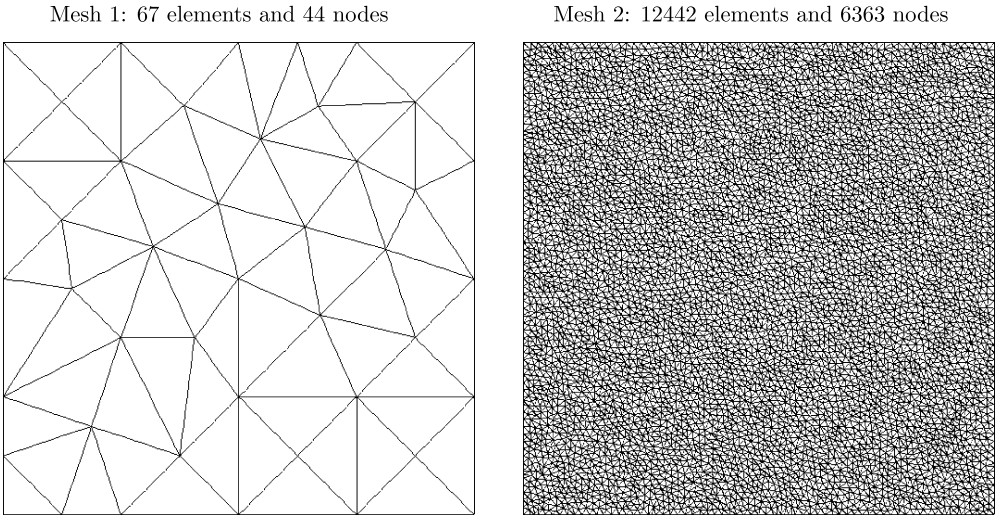

Fig. 2. Meshes used in the partition of unity finite element method (left) and the conventional finite element method (right) for the accuracy test problem.

Table 1
Relative errors obtained using Iso-PUFEM, Aniso-PUFEM, and FEM on a mesh with 67 elements and 44 nodes for the accuracy test problem using different numbers of enrichments Q and $\Delta t = 10^{-5}$ at finite time $t = 10^{-3}$.

	Q						
	1	2	3	4	5	6	7
Iso-PUFEM	2.47E-01	1.41E-01	7.47E-02	6.67E-02	6.37E-02	5.96E-02	5.90E-02
Aniso-PUFEM	4.59E-02	1.40E-02	8.30E-03	6.81E-03	6.62E-03	6.55E-03	6.45E-03
FEM	6.53E-03	6.53E-03	6.53E-03	6.53E-03	6.53E-03	6.53E-03	6.53E-03

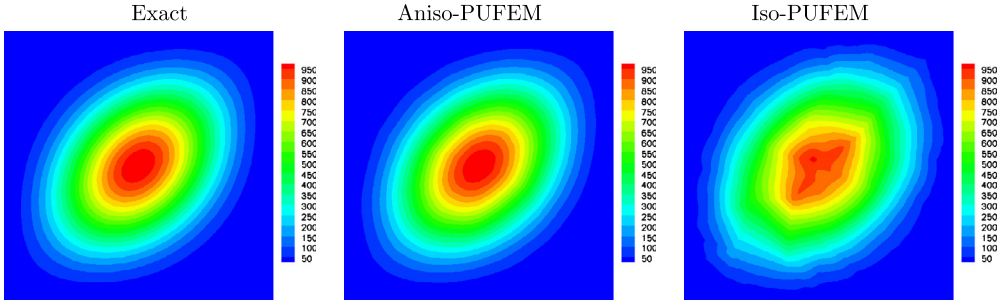

Fig. 3. Analytical solution (left), Aniso-PUFEM solution with $Q = 3$ (middle) and Iso-PUFEM solution with $Q = 7$ (right) on a coarse mesh for the accuracy test problem at time $t = 10^{-3}$.

that the first and second plots are almost identical. However, the approximation obtained using the standard Gaussian enrichments shows a significantly poorer approximation. Furthermore, we display in Fig. 4 the radial cross-section of the solution along the line passing through the domain corners namely, the points with coordinates $(-1,-1)^{\top}$ and $(1,1)^{\top}$. The figure shows a comparison between the solutions obtained using the Aniso-PUFEM and those obtained using the Iso-PUFEM at time $t = 10^{-3}$. It is clear that Fig. 4 demonstrates the close match between the Aniso-PUFEM solution and the exact solution, with relatively large discrepancies in the Iso-PUFEM solution. However, it should also be noted that the isotropic Gaussian enrichments are still efficient at capturing the steep gradients of the solutions. This is reflected in the meaningful approximations that are achieved at a relatively small number of degrees of freedom. Moreover, Table 1 shows consistent improvements in the solution accuracy as the number of enrichment functions increases with both Aniso-PUFEM and Iso-PUFEM.

It should also be stressed that, when compared to the Aniso-PUFEM, the standard FEM yields an error of 6.53E-03 at the final time using 6363 degrees of freedom compared to an error of 8.30E-03 with only 132 degrees of freedom using the Aniso-PUFEM. Note that although both methods produce comparable accuracy, the Aniso-PUFEM requires only around 2% of the total number of degrees of freedom otherwise needed in the FEM. Hence, the proposed Aniso-PUFEM can achieve similar accuracy but with a significantly smaller number of degrees of freedom, thanks to the enrichment technique using functions that incorporate prior knowledge of the problem.

4.2. Diffusion problem with a single source

In our next example, we solve a transient anisotropic diffusion problem as described by (1) in the squared domain $[-1,1]^2$. However, now we choose a general source defined as

$$f(t,x,y) = \begin{cases} 1800, & \text{if} \quad (x,y) \in [-0.1,0.1]^2 \\ 300, & \text{otherwise} \end{cases}$$

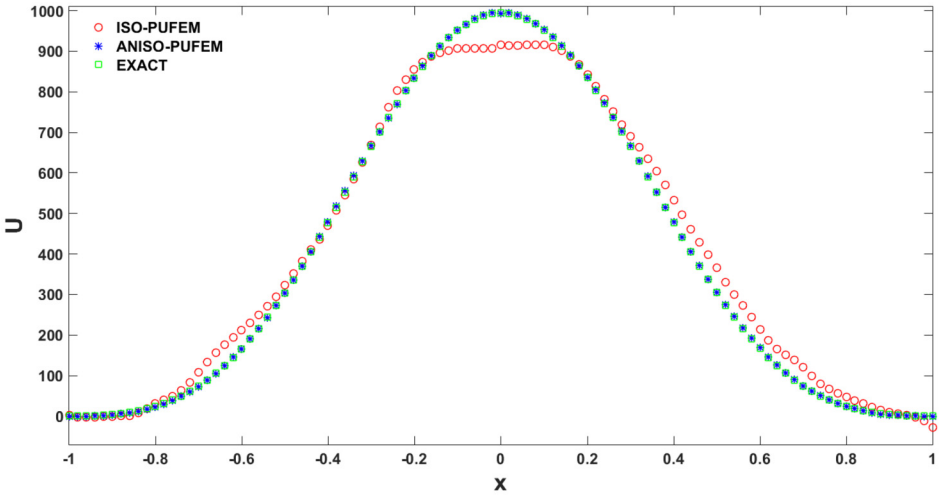

Fig. 4. Cross-section of the solutions in Fig. 3 along the main diagonal.

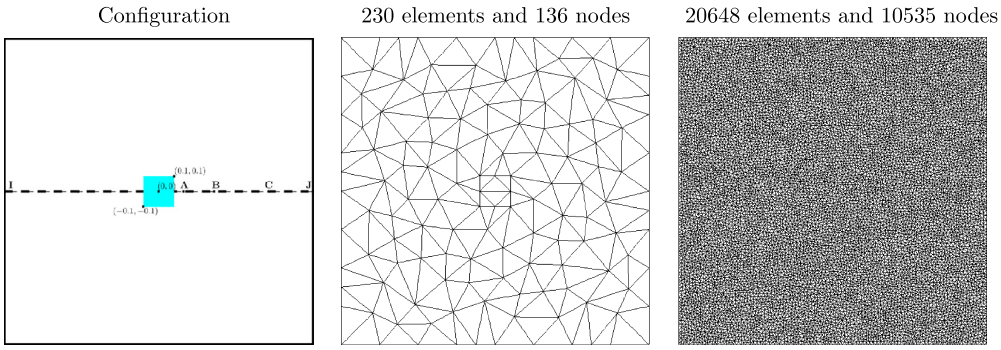

Fig. 5. Configuration (left), Mesh 1 (middle) and Mesh 2 (right) used for the diffusion problem with a single source.

Table 2
Time evolution of the solution at points A, B, and C for the diffusion problem with a single source.

# timesteps	Point A		Point B		Point C	
	FEM	Aniso-PUFEM	FEM	Aniso-PUFEM	FEM	Aniso-PUFEM
1	4.01	4.01	3.51	3.53	3.04	3.04
7	25.88	25.90	24.62	24.66	22.12	22.11
13	45.66	45.68	44.34	44.39	41.46	41.45
19	64.96	64.97	63.63	63.68	60.65	60.64
25	84.06	84.08	82.75	82.79	79.73	79.71
31	103.08	103.09	101.77	101.81	98.72	98.71
37	122.05	122.06	120.74	120.78	117.68	117.66
43	140.99	140.99	139.68	139.72	136.61	136.59
49	159.91	159.91	158.60	158.64	155.53	155.51

Fig. 5 shows the computational domain with a source located in its centre. In this example, the initial condition $u_0(x, y) = 0$, the boundary function $g(t, x, y) = 0$, the misalignment angle $\alpha = \frac{\pi}{16}$, and the diffusion coefficients $K_\perp = 1$ and $K_\parallel = 3$. Note that this problem does not have an analytical solution and must be solved numerically. To this end, the timestep is set at $\Delta t = 0.01$ and numerical results are presented at different times. Again, the problem is solved using the Aniso-PUFEM and the obtained results are compared to those obtained using the FEM. We consider two unstructured meshes with different element densities as shown in Fig. 5. A coarse mesh (Mesh 1) of 136 nodes is equipped with $Q = 6$ directional enrichment functions to calculate the Aniso-PUFEM solution. A very fine mesh (Mesh 2) is used with the standard FEM to calculate a reference solution for this example. The enrichment is centred at the origin *i.e.*, we choose $\mathbf{x}_0 = (0, 0)^\top$ in (13) which is also the centre of the domain.

The solution distributions obtained using the Aniso-PUFEM and FEM are illustrated in Fig. 6 where the numerical results are shown at three different time instants namely, $t = 0.01$, $t = 0.1$ and $t = 0.5$. It can be clearly seen from this figure that similar results are obtained using both methods. To facilitate the comparison of the results, a cross-section along the horizontal at $x = 0$ of solutions at time $t = 0.5$ is depicted in Fig. 6. The results obtained using the Aniso-PUFEM with $Q = 6$ exhibit similar solution trends to those obtained using the FEM. Furthermore, to assess the solution changes throughout the time domain for both methods, Table 2 presents the solution evolution captured by both methods at three different points for 49 timesteps up to $t = 0.5$. The considered points, A, B, and C are shown in Fig. 5. The solution values obtained at these three points are similar with at least three significant digits of agreement. These results indicate that both the FEM and Aniso-PUFEM capture the same dynamics of the solution and the

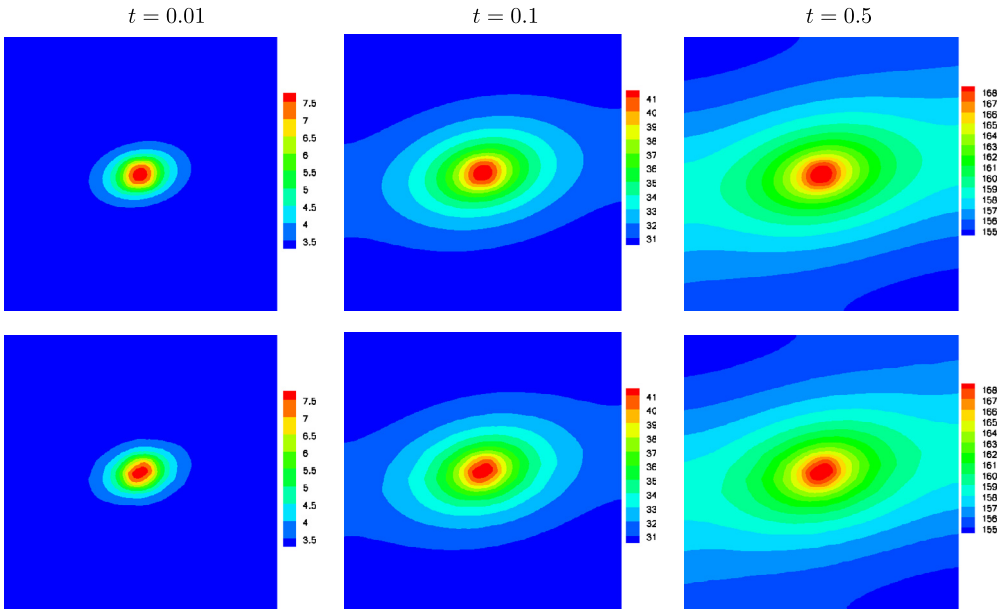

Fig. 6. Solutions obtained using the FEM on Mesh 2 (first row) and Aniso-PUFEM on Mesh 1 (second row) for the diffusion problem with a single source at three different instants $t = 0.01$, $t = 0.1$ and $t = 0.5$ from left to right.

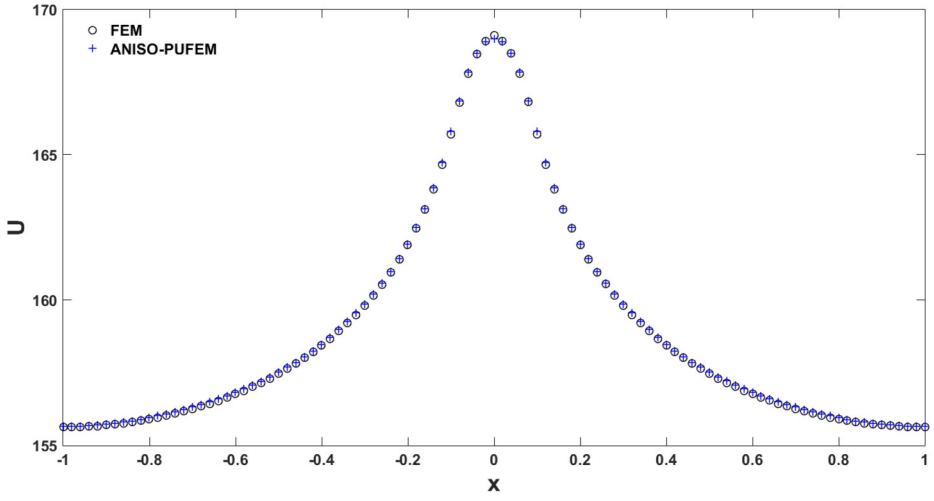

Fig. 7. Cross-section of the solution at $x = 0$ for the diffusion problem with a single source at time $t = 0.5$.

movement of solution fronts. However, it is worth noting that the FEM results are obtained using 10535 nodes or degrees of freedom, while the Aniso-PUFEM utilizes only $136 \times 6 = 816$ degrees of freedom. To evaluate the impact of the number of degrees of freedom on the computational cost, Table 3 summarizes the CPU time required in both methods to build the linear system of equations and solve it. The table demonstrates that the Aniso-PUFEM exhibits higher efficiency due to the low number of degrees of freedom. The Aniso-PUFEM results are obtained in approximately 64 seconds, with around 49 seconds spent on building the linear system and approximately 15 seconds on solving it. In contrast, the corresponding FEM results are obtained in approximately 546 seconds, with around 401 seconds spent on building the linear system and approximately 146 seconds on solving it. Therefore, the proposed Aniso-PUFEM achieves a similar accuracy with approximately 10% of the CPU time required in the conventional FEM (Fig. 7).

Table 3
Computational requirements in seconds for the FEM and Aniso-PUFEM solutions on the considered meshes with a number of enrichment functions $Q = 6$ and $\Delta t = 0.01$ for the diffusion problem with a single source.

	CPU time		
	Build	Solve	Total
FEM	400.89	145.48	546.37
Aniso-PUFEM	49.08	14.84	63.92

Our final concern in this example is to test the ability of the proposed Aniso-PUFEM to capture transient anisotropic diffusion for different values of the misalignment angle. Hence, we solve the problem using the same spatial and temporal discretization as before, but for three different misalignment angle $\alpha = \frac{3\pi}{4}$, $\alpha = \frac{\pi}{4}$ and $\alpha = 0$. Retaining the spatial discretization for the selected values of α would help assess the reliance of the Aniso-PUFEM on the chosen mesh. The same meshes used previously are retained for the new set of results, while all other parameters in the problem remain unchanged. Fig. 8 presents distributions of the solution obtained using the FEM and Aniso-PUFEM for the considered values of α at time $t = 0.5$. The plots show very similar patterns recovered using both methods, albeit with a much smaller number of

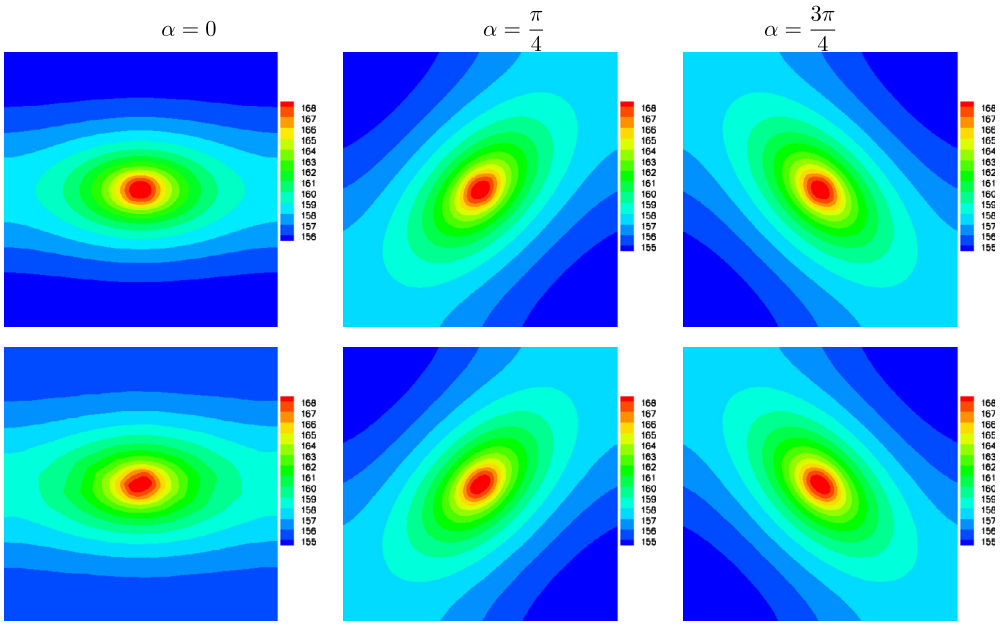

Fig. 8. Solutions obtained using the FEM on Mesh 2 (first row) and Aniso-PUFEM on Mesh 1 (second row) for the diffusion problem with a single source at time $t = 0.5$ for three different values of the misalignment angle $\alpha = 0$, $\frac{\pi}{4}$, and $\frac{3\pi}{4}$ from left to right.

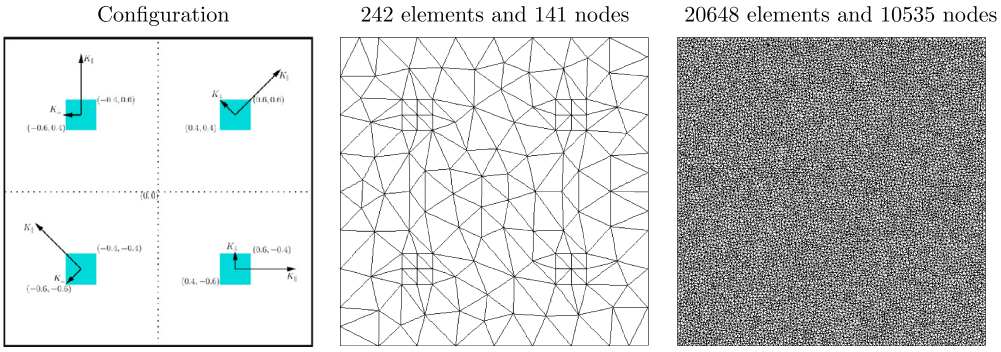

Fig. 9. Configuration (left), Mesh 1 (middle) and Mesh 2 (right) used for the diffusion problem with multiple sources.

degrees of freedom when using the Aniso-PUFEM. This similarity is observed in all cases, despite the coarse mesh used for the Aniso-PUFEM results. These findings suggest that the method is not sensitive to the mesh choice, thanks to incorporating the misalignment angle into the Aniso-PUFEM directional enrichment functions.

4.3. Diffusion problem with multiple sources

In this test example, we solve the same problem as before but with multiple sources. Again, the governing equations are given by the diffusion model (1) with the diffusion characteristics of the medium are taken to be similar to the previous example. However, we now assume four sources, the dimensions and location of which are shown in Fig. 9. The four embedded sources are defined as

$$f(t,x,y) = \begin{cases} 1800, & \text{if } |x-0.5| < 0.1 \text{ and } |y-0.5| < 0.1 \text{ and } t \le 0.2, \\ 1800, & \text{if } |x-0.5| < 0.1 \text{ and } |y+0.5| < 0.1 \text{ and } t \le 0.2, \\ 1800, & \text{if } |x+0.5| < 0.1 \text{ and } |y-0.5| < 0.1 \text{ and } t \le 0.2, \\ 1800, & \text{if } |x+0.5| < 0.1 \text{ and } |y+0.5| < 0.1 \text{ and } t \le 0.2, \\ 300, & \text{otherwise.} \end{cases}$$

In our simulation for this example, the misalignment angle $\alpha = \frac{5\pi}{4}$, the parallel and perpendicular coefficients for all sources are respectively $K_\perp = 1$ and $K_\parallel = 3$. In addition, the comparison study of this test example is designed similarly to the previous one, where two meshes are used with the reference solution based on a fine mesh and a FEM solution. Fig. 9 presents the two meshes considered in the simulations. In this example, the number of degrees of freedom in the reference solution is again 10535, while a much lower number is used for the Aniso-PUFEM, which is $846 = 141 \times 6$. The timestep is again taken as $\Delta t = 0.01$. It should be pointed out that to handle multiple sources in this example, each enrichment function is taken to be the sum of four exponential functions G_q that are of the same order q but centred at a different source. Thus, an exponential function is centred at each of the sources. In equation (13), we choose four different values for $\mathbf{x}_0$ to reconstruct the enrichment functions. The considered values are $(0.5, 0.5)$, $(-0.5, 0.5)$, $(0.5, -0.5)$ and $(-0.5, -0.5)$. The four exponential functions are then summed into one enrichment function for each order q.

Fig. 10 displays the solution distributions obtained using the Aniso-PUFEM on Mesh 1 compared to the reference solution at three considered instants $t = 0.01$, 0.1 and 0.2. As can be seen in this figure, the Aniso-PUFEM solution matches the reference solutions at all considered times. The symmetry in the Aniso-PUFEM solutions should also be noted in the presented results. It is important to highlight the significant difference in the number of degrees of freedom under the considered

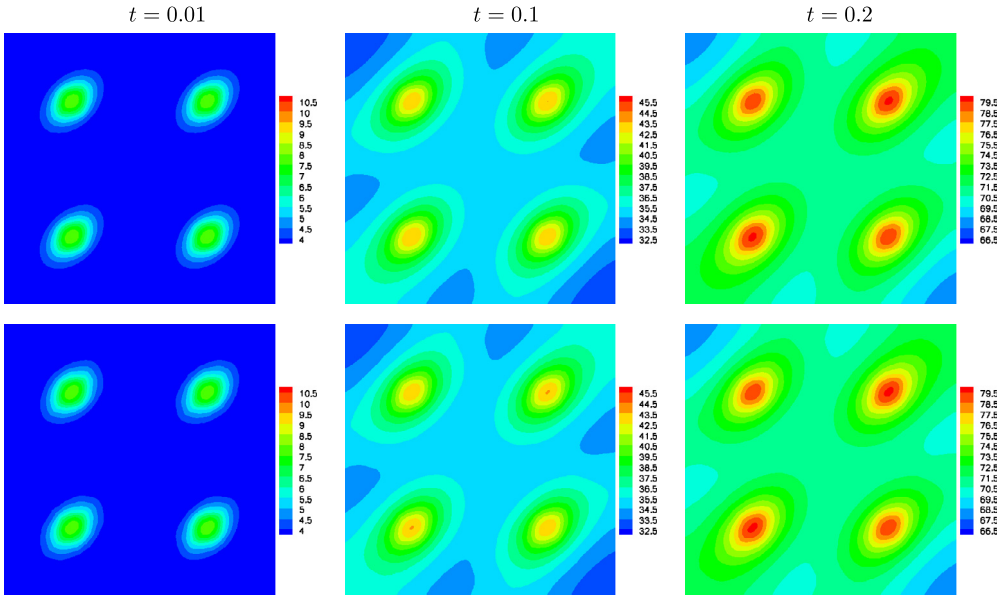

Fig. 10. Solutions obtained using the FEM on Mesh 2 (first row) and the Aniso-PUFEM on Mesh 1 (second row) for the diffusion problem with multiple sources with $\alpha = \frac{5\pi}{4}$ at three different instants $t = 0.01$, $t = 0.1$ and $t = 0.2$ from left to right.

Table 4
Computational requirements in seconds for the FEM and Aniso-PUFEM solutions on the considered meshes with a number of enrichment functions $Q = 6$ and $\Delta t = 0.01$ for the diffusion problem with multiple sources.

	CPU time		
	Build	Solve	Total
FEM	388.12	93.12	481.25
Aniso-PUFEM	27.29	5.31	32.60

diffusion conditions. The Aniso-PUFEM results are obtained with 864 degrees of freedom, whereas 10535 degrees of freedom are used in the FEM. Next we run the test again but this time with a reduced misalignment angle of $\alpha = \frac{\pi}{16}$, while keeping all other parameters unchanged. The new set of results is displayed in Fig. 11. This figure shows the solution distributions obtained using the Aniso-PUFEM compared to the reference solution at the time instants $t = 0.01$, 0.1 and 0.2. The Aniso-PUFEM results capture the same solution trends as those obtained using the FEM. It is evident that for the considered diffusion conditions, both the FEM and the Aniso-PUFEM accurately resolve the moving solution fronts and capture the solution dynamics. The reduced misalignment angle is clearly reflected in the diffusion patterns seen in this figure compared to Fig. 10. However, it is important to note that the FEM results are obtained on a fine mesh with 20648 elements and 10535 nodes, while the Aniso-PUFEM results are computed using a coarse mesh with 242 elements and 141 nodes, along with six enrichment functions. This significant reduction in the total number of degrees of freedom is also reflected in a corresponding reduction in the CPU time required. Table 4 presents the CPU time required for both solutions, showing the advantage of using the Aniso-PUFEM in terms of computational efficiency. We also observe that the same coarse mesh is retained here although the misalignment angle has changed. Nevertheless, the performance of the Aniso-PUFEM has not deteriorated thanks to the proposed directional enrichment functions.

Our last concern in this example is to assess the performance of the Aniso-PUFEM when the problem involves multiple misalignment angles. We reconsider the example where the angles associated with the sources are $\alpha = \frac{\pi}{4}, \frac{\pi}{2}, \frac{3\pi}{4}$ and 2π as illustrated in Fig. 9. All the remaining problem parameters are kept the same as before. The meshes used for the numerical solutions, as well as the number of enrichment functions, are also retained. Fig. 11 presents the solution obtained with the Aniso-PUFEM compared to the reference solution at $t = 0.01$, 0.1 and 0.2. The figure demonstrates the close match between the two solutions. Again it is important to highlight that the Aniso-PUFEM solution accurately captures the different misalignment angles without the need to change the mesh. This flexibility is achieved through the directional enrichment functions which can adapt to changes in the misalignment.

4.4. Diffusion problem in a circular domain

In the last test example, we solve an anisotropic diffusion problem with multiple heat sources in a circular geometry. The computational domain is a circle centred at the origin with a unit radius as shown in Fig. 12. In this example, four embedded heat sources are considered and two different cases are examined separately. In the first case, all four sources dissipate the same amount of heat with the heat sources defined as

$$f(t,x,y) = \begin{cases} 1800, & \text{if } |x-0.5| < 0.1 \text{ and } |y-0.5| < 0.1 \text{ and } t \le 0.2, \\ 1800, & \text{if } |x-0.5| < 0.1 \text{ and } |y+0.5| < 0.1 \text{ and } t \le 0.2, \\ 1800, & \text{if } |x+0.5| < 0.1 \text{ and } |y-0.5| < 0.1 \text{ and } t \le 0.2, \\ 1800, & \text{if } |x+0.5| < 0.1 \text{ and } |y+0.5| < 0.1 \text{ and } t \le 0.2, \\ 300, & \text{otherwise.} \end{cases} \tag{23}$$

In the second case, the sources dissipate different amounts of heat. The heat sources are given by:

$$f(t,x,y) = \begin{cases} 1300, & \text{if } |x-0.5| < 0.1 \text{ and } |y-0.5| < 0.1 \text{ and } t \le 0.2, \\ 2300, & \text{if } |x-0.5| < 0.1 \text{ and } |y+0.5| < 0.1 \text{ and } t \le 0.2, \\ 2800, & \text{if } |x+0.5| < 0.1 \text{ and } |y-0.5| < 0.1 \text{ and } t \le 0.2, \\ 1800, & \text{if } |x+0.5| < 0.1 \text{ and } |y+0.5| < 0.1 \text{ and } t \le 0.2, \\ 300, & \text{otherwise.} \end{cases} \tag{24}$$

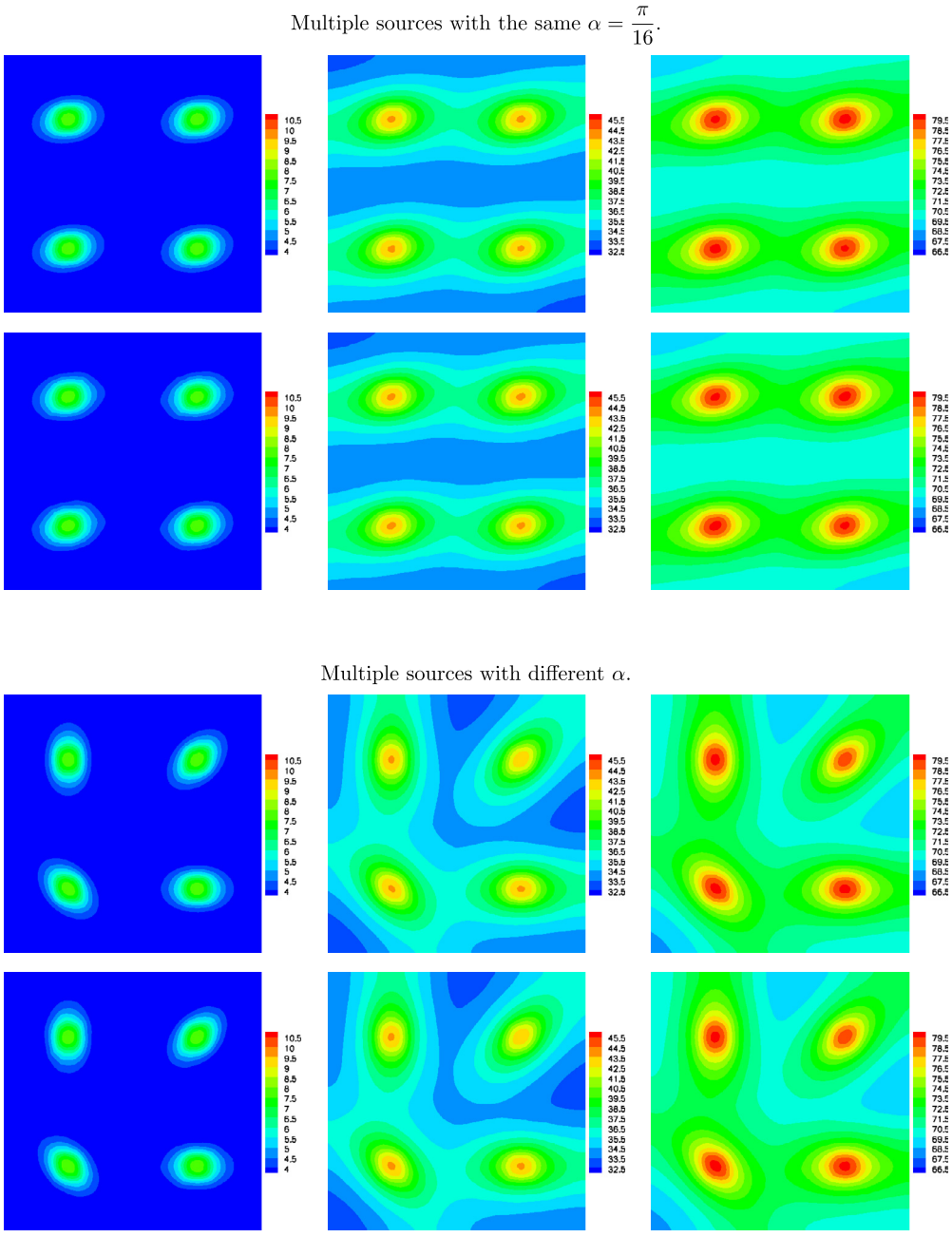

Fig. 11. Solutions obtained using the FEM on Mesh 2 (first and third rows) and the Aniso-PUFEM on Mesh 1 (second and fourth rows) at three different instants $t = 0.01$, $t = 0.1$ and $t = 0.2$ from left to right. Here, the top half shows the results obtained with the same α while the bottom half shows the results for sources with different α.

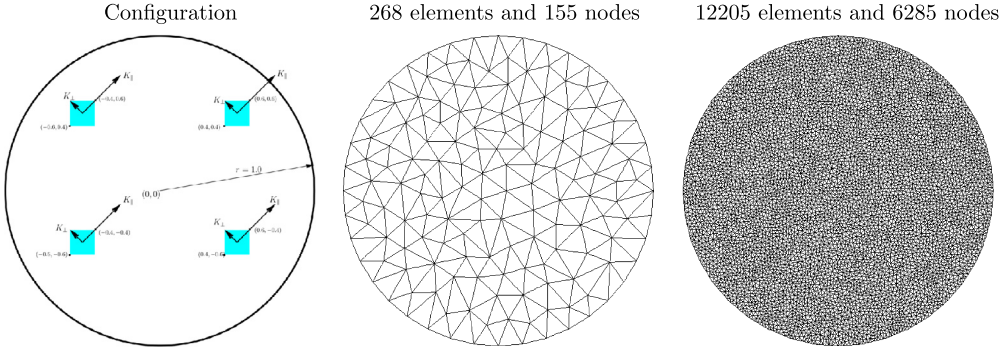

Fig. 12. Configuration (left), Mesh 1 (middle) and Mesh 2 (right) used for the diffusion problem in a circular domain.

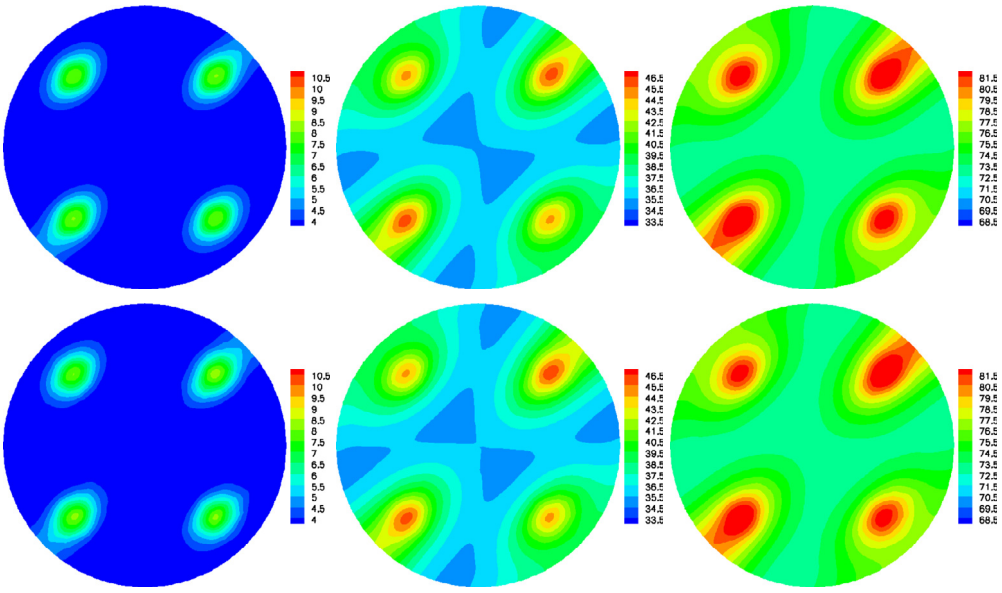

Case 2: Non-uniform heat sources defined in (24).

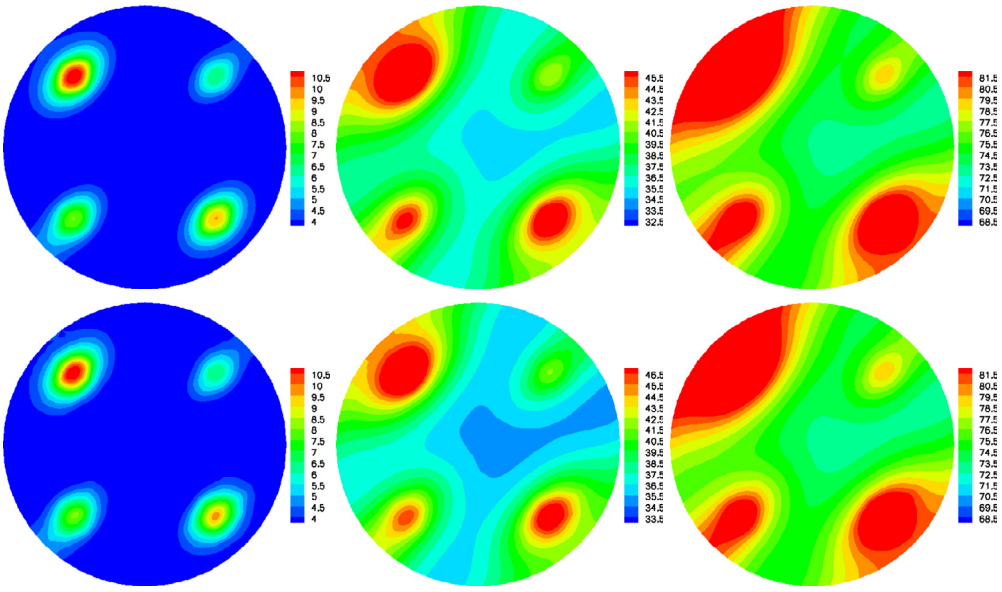

Fig. 13. Multi-heat sources on a circular domain: Temperature distributions obtained using the FEM on Mesh 2 (first row) and using the Aniso-PUFEM on Mesh 1 (second row) for two-dimensional heterogeneous anisotropic transient diffusion problems with four sources in a circular domain at three different instants.

As a consequence of this selection, the symmetry is not preserved in the solution field in the second case. In our simulations for both cases, the misalignment angle is set to $\alpha = \frac{\pi}{4}$ as demonstrated in Fig. 12, the parallel and perpendicular diffusion coefficients are $K_{\perp} = 1$ and $K_{\parallel} = 3$, respectively.

Similar to the previous test examples, the conventional FEM is used to create a reference solution using an h-refinement convergence study. It should be mentioned that the results obtained in this convergence study confirm the conclusions made in the previous examples, that the proposed Aniso-PUFEM yields a significant reduction in the total number of degrees of freedom compared to the conventional FEM. However, it is important to note that measuring the error using a numerically refined mesh for the reference solution will yield a more accurate representation of the geometry compared to the coarse mesh used in the Aniso-PUFEM. In all simulations carried out in this section, the unstructured meshes were generated using Triangle software [59]. For the finite element mesh, the element size h is refined in the range from 0.0003 to 0.0005. A comparatively larger size h in the range from 0.018 to 0.09 was employed in the Aniso-PUFEM to ensure convergence in the numerical solutions. The FEM reference solution is obtained on a dense mesh composed of 12205 elements and 6285 nodes, and it is used for qualitative comparisons with the Aniso-PUFEM solution. On the other hand, the Aniso-PUFEM solution is obtained on a coarse mesh of 268 elements and 155 nodes. For illustrative purposes, the two considered meshes are displayed in Fig. 12. Following a q-refinement convergence study, where we increase the number of enrichment functions until the Aniso-PUFEM solution converges, it is achieved using $Q = 4$ in the enrichment functions. The time domain in both solutions is discretized using $\Delta t = 0.01$ and the obtained solutions are presented at three different instants.

Fig. 13 depicts the results obtained for the two considered cases using the conventional FEM and the proposed Aniso-PUFEM at three

different instances, namely, $t = 0.01$, 0.1, and 0.2. The solution snapshots demonstrate that similar heat patterns are obtained with both methods at all times and in both cases. The results are consistent with the conclusions made in previous test examples. Despite the close similarities, the Aniso-PUFEM solutions show a significant improvement in efficiency compared to the standard FEM. In the first case, we observe the preserved symmetry when using equivalent heat sources in the simulation. As expected, this symmetry is disturbed in the second case. Furthermore, for different values of temperature at the sources, the thermal fronts travel faster towards the domain boundary. The results in this diffusion problem confirm our previous conclusions on the accuracy and efficiency of the proposed Aniso-PUFEM and reveal its ability in dealing with complicated and non-symmetric heat patterns. It should be noted that despite the large difference between the number of degrees of freedom used in the Aniso-PUFEM and the FEM, both methods produced similar results. Therefore one may conclude that the proposed Aniso-PUFEM performs very well for the anisotropic diffusion on this enclosure and it resolves all the solution features without the need for refined meshes in the simulations.

5. Conclusion

In this study, we proposed a novel approach for solving anisotropic diffusion problems using an enriched finite element method. The primary objective is to achieve accurate solutions while improving approximation efficiency and leveraging the advantages of the conventional finite element method. For the spatial discretization, we employ the partition of unity finite element method, while an implicit technique is implemented for the time integration. To enhance the approximation properties of the finite element method, we introduced exponential functions as enrichments. These functions incorporate the misalignment angle, capturing the solution behaviour with steep gradients. Consequently, the accuracy of the numerical approximation is significantly improved even on coarse meshes. The incorporation of these directional enrichment functions not only leverages a priori knowledge about the problem but also allow for adaptability to changes in the misalignment angle without the need for remeshing. This adaptability is a valuable feature, as it ensures that the method remains independent on the mesh. This feature further enhances the applicability and versatility of our approach. In addition, the proposed approach demonstrates remarkable improvements in approximation efficiency, requiring significantly fewer degrees of freedom compared to the standard finite element method. Moreover, the directional enrichment functions can adapt to the changes in the misalignment angle, accommodating multiple steepness levels in the solutions and various directions of misalignment.

Extensive numerical results consistently demonstrate the efficiency of our proposed method in achieving the desired levels of accuracy. Comparisons to the conventional finite element method and other enrichments, showcase significant improvements in the efficiency of the proposed enrichments. For the considered anisotropic diffusion problems, the proposed method achieves the same level of accuracy as the standard finite element method but it utilizes only 10% of the number of degrees of freedom. This reduction in the computational cost makes our approach practical for solving complex anisotropic transient diffusion problems. In fact, compared to other enrichments with a similar number of degrees of freedom, our method achieves an order of magnitude improvement. The proposed partition of unity finite element method not only provides reliable and precise solutions but also extends the capabilities of the finite element method to effectively address aspects of anisotropic diffusion problems that were previously considered ineffective using this method. It should be stressed that the partition of unity finite element method enables using large elements to retrieve steep solution gradients and moving fronts without the need for small elements. However, requiring a highly accurate geometry representation may require the use of small elements. Therefore, it would be very useful in future developments to consider an Isogeometric partition of unity finite element method for which non-uniform rational basis spline can be implemented to exactly represent the geometry on a coarse mesh while capturing the steep solution gradients and moving fronts with the proposed anisotropic enrichments. In such situations, dense refined meshes can be avoided. Future work will also focus on developing adaptive enrichments based on an error estimator for anisotropic diffusion and extension of these approaches to conduction-radiation models in anisotropic three-dimensional domains.

Data availability

Data will be made available on request.

References

[1] I. Aavatsmark, T. Barkve, Ø. Bøe, T. Mannseth, Discretization on non-orthogonal, quadrilateral grids for inhomogeneous, anisotropic media, J. Comput. Phys. 127 (1) (1996) 2–14.
[2] I. Aavatsmark, T. Barkve, Ø. Bøe, T. Mannseth, Discretization on unstructured grids for inhomogeneous, anisotropic media. Part II: discussion and numerical results, SIAM J. Sci. Comput. 19 (5) (1998) 1717–1736.
[3] M.L. Adams, Discontinuous finite element transport solutions in thick diffusive problems, Nucl. Sci. Eng. 137 (3) (2001) 298–333.
[4] B. Andreianov, F. Boyer, F. Hubert, Discrete duality finite volume schemes for Leray-Lions-type elliptic problems on general 2d meshes, Numer. Methods Partial Differ. Equ. 23 (1) (2007) 145–195.
[5] P. Anguill, P. Cargo, C. Énaux, P. Hoch, E. Labourasse, G. Samba, An asymptotic preserving method for the linear transport equation on general meshes, J. Comput. Phys. 450 (2022) 110859.
[6] C. Aricò, T. Tucciarelli, Monotonic solution of heterogeneous anisotropic diffusion problems, J. Comput. Phys. 252 (2013) 219–249.
[7] J. Bonelle, A. Ern, Analysis of compatible discrete operator schemes for elliptic problems on polyhedral meshes, ESAIM: Math. Model. Numer. Anal. 48 (2) (2014) 553–581.
[8] C. Buet, B. Despres, G. Morel, Trefftz discontinuous Galerkin basis functions for a class of Friedrichs systems coming from linear transport, Adv. Comput. Math. 46 (3) (2020) 1–27.
[9] F. Chaland, G. Samba, Discrete ordinates method for the transport equation preserving one-dimensional spherical symmetry in two-dimensional cylindrical geometry, Nucl. Sci. Eng. 182 (4) (2016) 417–434.
[10] A.S. Chamarthi, H. Nishikawa, K. Komurasaki, First order hyperbolic approach for anisotropic diffusion equation, J. Comput. Phys. 396 (2019) 243–263.
[11] C.A. Chavez, N.O. Moraga, C.H. Salinas, R.C. Cabrales, R.A. Ananias, Modeling unsteady heat and mass transfer with prediction of mechanical stresses in wood drying, Int. Commun. Heat Mass Transf. 123 (2021) 105230.
[12] K. Christodoulou, O. Laghrouche, M.S. Mohamed, J. Trevelyan, High-order finite elements for the solution of Helmholtz problems, Comput. Struct. 191 (2017) 129–139.
[13] O. Coulaud, A. Loseille, P. Schrooyen, Anisotropic mesh adaptation for high-order finite elements spaces with the log-simplex method. Application to discontinuous Galerkin methods, J. Comput. Phys. (2024) 112774.
[14] N. Dahmen, J. Droniou, F. Rogier, A cost-effective nonlinear extremum-preserving finite volume scheme for highly anisotropic diffusion on Cartesian grids, with application to radiation belt dynamics, J. Comput. Phys. 463 (2022) 111258.
[15] P. Degond, F. Deluzet, C. Negulescu, An asymptotic preserving scheme for strongly anisotropic elliptic problems, Multiscale Model. Simul. 8 (2) (2010) 645–666.
[16] P. Degond, A. Lozinski, J. Narski, C. Negulescu, An asymptotic-preserving method for highly anisotropic elliptic equations based on a micro–macro decomposition, J. Comput. Phys. 231 (7) (2012) 2724–2740.
[17] L. Degtyarev, S. Medvedev, Methods for numerical simulation of ideal mhd stability of axisymmetric plasmas, Comput. Phys. Commun. 43 (1) (1986) 29–56.
[18] F. Dell'Accio, F. Di Tommaso, A. Guessab, F. Nudo, Enrichment strategies for the simplicial linear finite elements, Appl. Math. Comput. 451 (2023) 128023.
[19] F. Dell'Accio, F. Di Tommaso, A. Guessab, F. Nudo, A general class of enriched methods for the simplicial linear finite elements, Appl. Math. Comput. (2023) 128149.
[20] G. Diwan, M. Mohamed, M. Seaid, J. Trevelyan, O. Laghrouche, Mixed enrichment for the finite element method in heterogeneous media, Int. J. Numer. Methods Eng. 101 (2015) 54–78.
[21] G.C. Diwan, M.S. Mohamed, Pollution studies for high order isogeometric analysis and finite element for acoustic problems, Comput. Methods Appl. Mech. Eng. 350 (2019) 701–718.
[22] G.C. Diwan, M.S. Mohamed, Iterative solution with shifted Laplace preconditioner for plane wave enriched isogeometric analysis and finite element discretization for high-frequency acoustics, Comput. Methods Appl. Mech. Eng. 384 (2021) 114006.
[23] J. Droniou, R. Eymard, A mixed finite volume scheme for anisotropic diffusion problems on any grid, Numer. Math. 105 (1) (2006) 35–71.

[24] J. Droniou, R. Eymard, T. Gallouët, R. Herbin, A unified approach to mimetic finite difference, hybrid finite volume and mixed finite volume methods, Math. Models Methods Appl. Sci. 20 (02) (2010) 265–295.
[25] M.G. Edwards, C.F. Rogers, Finite volume discretization with imposed flux continuity for the general tensor pressure equation, Comput. Geosci. 2 (4) (1998) 259–290.
[26] S. Eisenträger, E. Atroshchenko, R. Makvandi, On the condition number of high order finite element methods: influence of p-refinement and mesh distortion, Comput. Math. Appl. 80 (11) (2020) 2289–2339.
[27] A. El Kahoui, M. Malek, N. Izem, M. Shadi Mohamed, M. Seaid, Partition of unity finite element analysis of nonlinear transient diffusion problems using p-version refinement, Comput. Model. Eng. Sci. 124 (1) (2020) 61–78.
[28] B. van Es, Numerical Methods for Anisotropic Diffusion, Technische Universiteit, Eindhoven, 2015.
[29] R. Eymard, T. Gallouet, R. Herbin, Discretization of heterogeneous and anisotropic diffusion problems on general nonconforming meshes SUSHI: a scheme using stabilization and hybrid interfaces, IMA J. Numer. Anal. 30 (4) (2009) 1009–1043.
[30] G. Galindez-Ramirez, F. Contreras, D. Carvalho, P. Lyra, A very high-order flux reconstruction approach coupled to the mpfa-ql finite volume method for the numerical simulation of oil-water flows in 2d petroleum reservoirs, Appl. Math. Model. 106 (2022) 799–821.
[31] R. Geelen, J. Plews, J. Dolbow, Scale-bridging with the extended/generalized finite element method for linear elastodynamics, Comput. Mech. 68 (2) (2021) 295–310.
[32] G. Giorgiani, H. Bufferand, F. Schwander, E. Serre, P. Tamain, A high-order non field-aligned approach for the discretization of strongly anisotropic diffusion operators in magnetic fusion, Comput. Phys. Commun. 254 (2020) 107375.
[33] D. Green, X. Hu, J. Lore, L. Mu, M.L. Stowell, An efficient high-order numerical solver for diffusion equations with strong anisotropy, Comput. Phys. Commun. 276 (2022) 108333.
[34] A. Guessab, Y. Zaim, A unified and general framework for enriching finite element approximations, in: Progress in Approximation Theory and Applicable Complex Analysis: In Memory of QI Rahman, 2017, pp. 491–519.
[35] S.R. Hejazi, E. Saberi, F. Mohammadizadeh, Anisotropic non-linear time-fractional diffusion equation with a source term: classification via Lie point symmetries, analytic solutions and numerical simulation, Appl. Math. Comput. 391 (2021) 125652.
[36] M. Held, M. Wiesenberger, A. Stegmeir, Three discontinuous Galerkin schemes for the anisotropic heat conduction equation on non-aligned grids, Comput. Phys. Commun. 199 (2016) 29–39.
[37] J. Hu, S. Jin, Q. Li, Asymptotic-Preserving Schemes for Multiscale Hyperbolic and Kinetic Equations, Handbook of Numerical Analysis, vol. 18, Elsevier, 2017, pp. 103–129.
[38] J. Jiang, M. Shadi Mohamed, M. Seaid, H. Li, Fast inverse solver for identifying the diffusion coefficient in time-dependent problems using noisy data, Arch. Appl. Mech. 91 (4) (2021) 1623–1639.
[39] S. Jin, Asymptotic preserving (ap) schemes for multiscale kinetic and hyperbolic equations: a review, in: Lecture Notes for Summer School on Methods and Models of Kinetic Theory (M&MKT) Porto Ercole, Grosseto, Italy, 2010, pp. 177–216.
[40] D. Kuzmin, M. Shashkov, D. Svyatskiy, A constrained finite element method satisfying the discrete maximum principle for anisotropic diffusion problems, J. Comput. Phys. 228 (9) (2009) 3448–3463.
[41] C. Le Potier, H. Thanh, A cell-centered scheme for heterogeneous anisotropic diffusion problems on general meshes, Int. J. Finite Vol. (2012) 1–40.
[42] N.-S. Lee, K.-J. Bathe, Effects of element distortions on the performance of isoparametric elements, Int. J. Numer. Methods Eng. 36 (20) (1993) 3553–3576.
[43] K. Lipnikov, D. Svyatskiy, Y. Vassilevski, A monotone finite volume method for advection–diffusion equations on unstructured polygonal meshes, J. Comput. Phys. 229 (11) (2010) 4017–4032.
[44] M. Malek, N. Izem, M.S. Mohamed, M. Seaid, M. Wakrim, Numerical solution of Rosseland model for transient thermal radiation in non-grey optically thick media using enriched basis functions, Math. Comput. Simul. 180 (2021) 258–275.
[45] M. Malek, N. Izem, M. Seaid, M.S. Mohamed, M. Wakrim, A partition of unity finite element method for nonlinear transient diffusion problems in heterogeneous materials, Comput. Appl. Math. 38 (2) (2019) 1–19.
[46] R. Marchand, M. Dumberry, Carre: a quasi-orthogonal mesh generator for 2d edge plasma modelling, Comput. Phys. Commun. 96 (2) (1996) 232–246.
[47] J. Marsden, A. Weinstein, Calculus I, Springer Science & Business Media, 1985.
[48] E. Meier, V. Lukin, U. Shumlak, Spectral element spatial discretization error in solving highly anisotropic heat conduction equation, Comput. Phys. Commun. 181 (5) (2010) 837–841.
[49] J. Melenk, I. Babuška, The partition of unity finite element method: basic theory and applications, Comput. Methods Appl. Mech. Eng. 139 (1996) 289–314.
[50] M. Mohamed, M. Seaid, J. Trevelyan, O. Laghrouche, A partition of unity fem for time-dependent diffusion problems using multiple enrichment functions, Int. J. Numer. Methods Eng. 93 (2013) 245–265.
[51] M. Mohamed, M. Seaid, J. Trevelyan, O. Laghrouche, Time-independent hybrid enrichment for finite element solution of transient conduction-radiation in diffusive grey media, J. Comput. Phys. 251 (2013) 81–101.
[52] M. Mohamed, M. Seaid, J. Trevelyan, O. Laghrouche, An enriched finite element model with q-refinement for radiative boundary layers in glass cooling, J. Comput. Phys. 258 (2014) 718–737.
[53] M.S. Mohamed, M. Seaid, A. Bouhamidi, Iterative solvers for generalized finite element solution of boundary-value problems, Numer. Linear Algebra Appl. 25 (6) (2018) e2205.
[54] H. Nordanger, A. Morozov, J. Stenhammar, Anisotropic diffusion of ellipsoidal tracers in microswimmer suspensions, Phys. Rev. Fluids 7 (1) (2022) 013103.
[55] J. Pasdunkorale A, I.W. Turner, A second order control-volume finite-element least-squares strategy for simulating diffusion in strongly anisotropic media, Appl. Comput. Math. (2005) 1–16.
[56] A. Raees, M. Raees-ul Haq, H. Xu, Q. Sun, Three-dimensional stagnation flow of a nanofluid containing both nanoparticles and microorganisms on a moving surface with anisotropic slip, Appl. Math. Model. 40 (5–6) (2016) 4136–4150.
[57] F. Semeraro, J.C. Ferguson, M. Acin, F. Panerai, N.N. Mansour, Anisotropic analysis of fibrous and woven materials part 2: computation of effective conductivity, Comput. Mater. Sci. 186 (2021) 109956.
[58] P. Sharma, G.W. Hammett, Preserving monotonicity in anisotropic diffusion, J. Comput. Phys. 227 (1) (2007) 123–142.
[59] J.R. Shewchuk, Triangle: engineering a 2d quality mesh generator and Delaunay triangulator, in: Workshop on Applied Computational Geometry, Springer, 1996, pp. 203–222.
[60] Z.-C. Shi, Nonconforming finite element methods, J. Comput. Appl. Math. 149 (1) (2002) 221–225.
[61] T. Shilt, P.J. O'Hara, J.J. McNamara, Stabilization of advection dominated problems through a generalized finite element method, Comput. Methods Appl. Mech. Eng. 383 (2021) 113889.
[62] C. Sovinec, A. Glasser, T. Gianakon, D. Barnes, R. Nebel, S. Kruger, D. Schnack, S. Plimpton, A. Tarditi, M. Chu, Nonlinear magnetohydrodynamics simulation using high-order finite elements, J. Comput. Phys. 195 (1) (2004) 355–386.
[63] S. Su, Q. Dong, J. Wu, A decoupled and positivity-preserving discrete duality finite volume scheme for anisotropic diffusion problems on general polygonal meshes, J. Comput. Phys. 372 (2018) 773–798.
[64] K.M. Terekhov, B.T. Mallison, H.A. Tchelepi, Cell-centered nonlinear finite-volume methods for the heterogeneous anisotropic diffusion problem, J. Comput. Phys. 330 (2017) 245–267.
[65] B. van Es, B. Koren, H.J. de Blank, Finite-difference schemes for anisotropic diffusion, J. Comput. Phys. 272 (2014) 526–549.
[66] L.R. Van Loon, J.M. Soler, W. Müller, M.H. Bradbury, Anisotropic diffusion in layered argillaceous rocks: a case study with Opalinus Clay, Environ. Sci. Technol. 38 (21) (2004) 5721–5728.
[67] H. Yang, B. Yu, Y. Li, G. Yuan, Monotonicity correction for second order element finite volume methods of anisotropic diffusion problems, J. Comput. Phys. 449 (2022) 110759.
[68] W. Zhan, X. Rao, H. Zhao, H. Zhang, S. Hu, W. Dai, Generalized finite difference method (gfdm) based analysis for subsurface flow problems in anisotropic formation, Eng. Anal. Bound. Elem. 140 (2022) 48–58.